Journal of Corrosion and Materials
www.corromat.com

J. Corros. Mater. (2024) 3(1), 67–82.

Shear-Activated Thickness Response in Entropy-Constrained Textured $BaTiO_3$ Polycrystals

Josef Michl[1,*], Sophie Tremblay[2]

[1] *Institute of Organic Chemistry and Biochemistry of the Czech Academy of Sciences, Praha, Czech Republic*
[2] *Department of Mechanical Engineering, Faculty of Applied Science, University of British Columbia, Vancouver, British Columbia V6T 1Z4, Canada.*

[*]Corresponding author: josef.michl@colorado.edu
[2]jsophietremblay527@gmail.com

(Received: 3 March 2024. Received in revised form: 25 May 2024. Accepted: 10 June 2024. Published online: 30 June 2024.)

Abstract

Flexoelectric polarization effects in dielectric ceramics depend on the strain gradient and are thus critical in microstructured, bent, indented, stacked, and miniaturized electromechanical devices. The flexoelectric properties of polycrystalline $BaTiO_3$ are determined not only by the numerical value of the flexoelectric coefficients but also by the orientation distribution through which each tensor entry is projected from its crystallographic expression to the coordinate frame of the material. A feasible orientation transfer process is designed for cubic $BaTiO_3$ polycrystals. Using the complete set of tabulated DFT and LDA flexoelectric tensors of $BaTiO_3$ crystals, the four-order flexoelectric tensor is rotated into the specimen coordinate frame, oriented according to the aligned, zero-tilt fiber, tilted-fiber, and isotropic orientations. An entropy-penalty function ensures that the orientation distribution is neither too narrowly peaked nor outside the realistic fabrication range. The tensor-channel transfer capability of an orientation-dependent texture is evaluated based on whether a finite-width tilted fiber texture can yield a stronger thickness-mode coefficient compared with perfectly aligned or isotropic states through the transfer of a predominantly shear-based crystallographic tensor entry. This is indeed the case for both coefficient sets. For the DFT flexoelectric tensor, the value of the thickness-mode coefficient increases from 0.360 nC m^{-1} in the aligned state to 0.954 nC m^{-1} in the tilted fiber texture. For the LDA tensor, the same texture transforms the coefficient from 0.150 nC m^{-1} to -5.088 nC m^{-1}, resulting in a 33.9-fold magnitude increase and a flip of polarity. Zero-tilt fiber causes a modulation of in-plane coefficients while leaving the thickness mode unaffected. Isotropic distribution averages the flexoelectric coefficients without retaining any preferential direction. Clearly, for flexoelectric materials, the optimization problem of texture engineering should be framed in terms of tensor-channel transfer.

Keywords: flexoelectricity; barium titanate; textured ceramics; orientation distribution function; tensor rotation; entropy regularization; polycrystal averaging; shear-channel transfer.

1. Introduction

A wide variety of functionality in ceramic materials results from interactions that are weak within a homogenous single crystal but are significant when coupled to structural features such as gradients, interfaces, finite size, and microstructure organization. Flexoelectricity is an illustrative example in this regard, in which the interaction is defined between polarization and strain gradients instead of uniform strains. Early crystal-physics work introduced flexoelectricity as a response to inhomogeneous deformation [1]. Mindlin's microstructure continuum framework supplied a mechanics basis for such inhomogeneous response [2]. Polarization-gradient theory then formalized the coupling in elastic dielectrics [3]. Tagantsev clarified the bulk flexoelectric effect in crystalline dielectrics [4]. Later thermodynamic analysis further established the symmetry setting of the effect [5]. Flexoelectricity has gained prominence in nanomaterials' electromechanics where substantial gradients exist close to surfaces, grain boundaries, cracks, pores, contacts, multilayer interfaces, and bending regions [6]. Nanoscale flexoelectricity further shows why small dimensions can amplify this coupling [7]. Ferroelectric thin-film and surface studies also connect flexoelectricity with finite-size electromechanical response [8]. Recent review literature confirms the importance of the effect in modern dielectric and ferroelectric systems [9]. Unlike regular piezoelectric effects, flexoelectric phenomena are generally not forbidden by any symmetry condition, even in centrosymmetric materials. The symmetry of flexoelectric coefficients therefore makes this coupling relevant for centrosymmetric ceramics [10].

It is possible to consider $BaTiO_3$ as a relevant framework for studying this problem in the context of flexoelectricity. The selected system is a well-known ceramic ferroelectric characterized by strong dielectric polarizability, which may exist in the paraelectric state with cubic symmetry, wherein piezoelectric coefficients equal zero by symmetry. It is therefore possible to focus on flexoelectricity in $BaTiO_3$ without accounting for possible contributions due to bulk piezoelectricity. $BaTiO_3$ and related titanate oxides are technologically important as materials for capacitor structures, sensors and actuators, thin dielectric layers, and lead-free dielectric applications [6]. Their relevance to nanoscale and surface-sensitive electromechanics has also been stressed in ferroelectric studies [8]. Broader review work confirms their importance for modern flexoelectric

materials design [9]. Experimental findings indicate that flexoelectric response exists in high-permittivity ceramics including $BaTiO_3$ [11]. Related measurements further demonstrate the relevance of flexoelectric effects in dielectric ceramics [12]. Atomistic theory connects the observed response with the intrinsic flexoelectric tensor [13]. First-principles calculations clarify the electronic and lattice-mediated contributions [14]. Finite-sample analysis shows that surface and boundary conditions may influence the observed response [15]. Modern first-principles theory further separates bulk, surface, and finite-field contributions [16]. These considerations suggest a modeling approach where the intrinsic crystallographic tensor is distinguished from the microstructure-based path via which it enters the specimen-level coefficient.

The polycrystalline case is particularly significant. Flexoelectric measurement in a ceramic material is not based on reading a single scalar out of a single crystal. Each crystallite hosts a fourth-order flexoelectric tensor in its crystallographic frame, and all of them contribute to the macroscopic response once their tensor is transformed into the specimen frame. Tensor transformation of anisotropic physical properties follows the general language of crystallographic tensors [17]. A random sample would probe all possible crystallographic orientations and approach an isotropic state, but a textured sample keeps some orientation memory of the fabrication process. Thus, texture becomes a true design parameter, comparable to grain size, porosity, phase fraction, domain state, and residual stress. Orientation distribution functions provide a standard representation of crystallographic texture [18]. Roe's formulation gives an early mathematical basis for representing orientation statistics [19]. Modern texture theory connects these distributions with anisotropy and processing history [20]. Statistical continuum theory supports the interpretation of microstructure averages as effective material behavior [21]. Self-consistent mechanics gives a related framework for estimating properties of heterogeneous aggregates [22]. Micromechanics of defects explains why local gradients and inhomogeneities can change effective response [23]. Random heterogeneous-material theory further connects microstructure organization with macroscopic properties [24]. In the case of flexoelectricity, the coupling mechanism has additional depth because a nominally longitudinal specimen tensor may receive contribution from crystallographic shear terms during transformation to the specimen frame.

The primary scientific question considered in this work is the following: Is it possible for a cubic ceramic with a finite-width tilted fiber texture to produce a larger flexoelectric effect in the thickness mode than either a perfectly oriented state or a completely isotropic sample through shear-channeling effect? This formulation of the problem is different from the usual quest for better texture since it assumes that the optimal ceramic will not necessarily be the one with the highest degree of axial orientation. Rather, the orientation distribution can be viewed as a channel transfer operator. Then, if the maximum contribution to the flexoelectric effect originates from shear-related coefficients, perfect orientation leaves a weaker channel along the device axis while the strong one remains unused. A deliberately tilted distribution may then be more effective than a perfectly aligned state.

The problem is applicable to ceramic processing, where even if one were to use some of the listed techniques such as tape casting, templated grain growth, hot forging, field-assisted sintering, directional solidification, and constrained grain growth, the resulting material would still have angular distribution since any method cannot guarantee a perfect state of orientation due to grain packing effects, localized boundary energy, abnormal grain growth, pore drag, and template misalignment. Thus, while an optimization problem based on selecting an infinitesimal value of entropy would yield a solution, its application might prove useless. Maximum-entropy reasoning provides a formal basis for avoiding unjustified concentration of probability mass [25]. Relative-entropy reasoning compares a selected distribution with a reference distribution [26]. Information-theoretic entropy also offers a general language for quantifying spread in probability distributions [27]. Large-deviation theory gives another mathematical context for the cost of concentrated probability states [28]. In the present formulation, relative entropy prevents overly concentrated textures and connects orientation optimization to a manufacturable texture range. As such, entropy is not merely a smoothing factor but a representation of the inherent orientation spread of real microstructures.

As for the numerical inputs, only those needed for tensor rotation have been listed in order to reduce redundancy. Specifically, the single crystal flexoelectric tensor for cubic $BaTiO_3$ was developed by using coefficients of longitudinal, transverse, and shear-related properties. Using the full set of coefficients obtained from Density Functional Theory and Local Density Approximation, the tensors were then subjected to rotation. Since the full set of coefficients cannot include the shear-related coefficient, only the experimental values listed in the coefficient table can be considered for use as scale factors. Tensor rotation is done for four cases of orientation – namely aligned, zero-tilt fiber, 49.1°-tilted fiber, and isotropic. This study aims at finding coefficients of the specimen frame, i.e., $\bar{\mu}_{1111}$, $\bar{\mu}_{1221}$, $\bar{\mu}_{1122}$, and $\bar{\mu}_{3333}$, especially $\bar{\mu}_{3333}$ which pertains to through-thickness deformation.

Contributions

The contributions of this work can be summarized as follows. First, the derivation distinguishes the effect of shear channel transfer in cubic $BaTiO_3$ from simple axial alignment. Second, it offers a replicable method for calculating tensorial rotations using the DFT/LDA data and four different orientation states. Third, it interprets the results as an engineering

design principle: the optimal crystal orientation for a flexoelectric ceramic material should be that which projects the dominant channel of the crystallographic tensor onto the strain gradient direction, and need not maximize any sort of crystallographic alignment.

2. Literature background and research position

Flexoelectric theory originated in the early treatment of polarization as a response to deformation inhomogeneity [1]. Microstructure-based continuum elasticity supplied an early mechanical basis for inhomogeneous deformation fields [2]. Polarization-gradient theory then established a continuum framework for strained elastic dielectrics [3]. Subsequent work by Tagantsev clarified the symmetry and thermodynamic considerations that characterize flexoelectric behavior in crystalline dielectrics [4]. Later analysis further explained why flexoelectricity is not restricted by the same inversion-symmetry requirement as piezoelectricity [5]. In particular, this work explains why $BaTiO_3$ is a viable flexoelectric candidate despite having no nonzero piezoelectric tensor components. It also explains why strain-gradient fields, rather than homogeneous strains, must be treated as the mechanical drivers of the response.

Modern developments in the field have been pursued along two interconnected lines of investigation. On the one hand, there is a strong emphasis on the experimental and device-scale consequences of flexoelectric phenomena. Significant flexoelectric polarizations were measured in ceramic dielectrics such as lead magnesium niobate [29]. Related measurements extended the evidence to other high-permittivity ceramic systems [30]. $BaTiO_3$ experiments further indicated the potential importance of strain-gradient polarization in high-permittivity ceramics [11]. Cross's work also stressed the practical importance of flexoelectricity in dielectric materials [12]. Review articles have emphasized flexoelectricity at the nanoscale and in strain-gradient electromechanics [6]. Ferroelectric surface and thin-film studies further connect the effect with finite-size and domain-structure dynamics [8]. A recent review consolidates the importance of flexoelectricity in modern materials design [9]. Spontaneous flexoelectric and flexomagnetic effects in nanoferroics also show how gradients and finite size can create functional responses [31]. The second approach involves atomistic and continuum calculations. Atomistic theory has been used to derive intrinsic flexoelectric tensor contributions [13]. First-principles work separated electronic and lattice-mediated responses [14]. Additional first-principles analysis extended the tensor-level interpretation [32]. Modern bulk flexoelectric theory clarified the boundary between bulk and surface contributions [16]. Density-functional perturbation analysis further refined the calculation of bulk flexoelectricity [33]. Computational homogenization has been used to treat strain-gradient and heterogeneity effects [34]. Finite-element studies have examined flexoelectricity in complex microstructural settings [35]. Phase-field and computational approaches have also been developed for strain-gradient electromechanical response [36].

From all of the above, we see that the observed response of a specimen does not represent a constant quantity at all. Rather, the observed response of a material to flexoelectric phenomena includes intrinsic values of bulk tensors, surface effects, dynamic contributions, electrostatic contributions, elastic boundary conditions, geometries of the electrodes, defects, and microstructure. Local measurements at crack tips show that strain gradient fields in the regions of rapid changes in strain can lead to substantial polarizations [37]. While such analysis can be useful when interpreting coefficients, it cannot directly help resolve the issue of texture design discussed above. When the single-crystal tensor has been found, one must perform orientation averaging to find what tensor elements contribute to the specimen coefficients.

Texture theory offers the means to formulate such an average. For polycrystals, orientation distribution functions express the distribution of crystal axes relative to those of a specimen. Bunge's texture theory establishes a framework linking pole figures and orientation distribution functions with probability densities in rotation space [18]. Roe's orientation-distribution formulation provides an earlier mathematical description of texture representation [19]. Texture and anisotropy theory connects such representations with crystallographic deformation and property response [20]. Flexoelectricity admits the same structure, albeit for higher-rank tensors with unusual index structures. The fourth-rank flexoelectric tensor includes longitudinal, transverse and shear-related flexoelectricity coefficients. Rotation acts on the tensor via products of four direction cosines. It follows that an orientation state that is less than ideal from an axial alignment standpoint can nonetheless be optimal in a certain specimen-frame coefficient if it maximizes the crystallographic channel's contribution to the relevant direction.

This is because of the hierarchy of flexoelectric coefficients in cubic $BaTiO_3$. The density functional theory set includes $\mu_{11} = -0.360$ nC m^{-1}, $\mu_{14} = 1.600$ nC m^{-1} and $\mu_{111} = -1.500$ nC m^{-1}. In turn, the local density approximation set includes $\mu_{11} = 0.150$ nC m^{-1}, $\mu_{14} = 1.904$ nC m^{-1} and $\mu_{111} = -5.460$ nC m^{-1}. Notably, the shear-related term is significantly larger in magnitude than the longitudinal term in the latter case. Therefore, a criterion for maximizing the axial $\bar{\mu}_{11}$ term would result in missing out on the dominant channel of flexoelectricity. The objective of this study is to examine whether tilted fiber texture can translate that shear effect into the effective $\bar{\mu}_{3333}$ response in a way that makes

sense in a finite width ceramic texture.

The entropy term differentiates this equation from optimization without such restrictions on rotations. Maximum-entropy reasoning is commonly employed to avoid overly narrow probability distributions when available information does not justify such concentration [25]. Relative entropy provides a direct measure for penalizing deviation from a chosen reference distribution [26]. Information theory gives the general mathematical foundation for this use of entropy in probability models [27]. In texture optimization, the entropy relative to an isotropic distribution acts as a regularizer on overly peaked orientations. Rather than deny the potential creation of highly peaked textures, it avoids returning an overly peaked orientation distribution because a fully singular distribution is not physically feasible for a sintered ceramic material. The result is a range of orientations balancing high sensitivity and physical manufacturability.

3. Constitutive formulation

Direct flexoelectric effect has the form of the equation with the components of the polarization vector P_i, strain tensor S_{jk} and coordinate x_l

$$P_i = \mu_{ijkl} \frac{\partial S_{jk}}{\partial x_l}. \tag{1}$$

Here, μ_{ijkl} is the fourth-order flexoelectric tensor. Since $S_{jk} = S_{kj}$, this tensor should have the minor symmetry property

$$\mu_{ijkl} = \mu_{ikjl}. \tag{2}$$

From a physical point of view, the relation given by (1) means that the electromechanical effect will be excited if there exists a nonuniformity of the strain field. Uniformly strained ceramics do not create the effect of direct flexoelectricity regardless of their dielectric and elastic energies; only varying strains produce polarization. This peculiarity should be considered while dealing with ceramic materials since local inhomogeneities appear around pores, surfaces, boundaries between phases, indenters, interfaces, etc. Another significant relation is the condition (2) which imposes restrictions on rotating tensors. The symmetry of the strain tensor lowers the number of independent tensor components but does not turn the flexoelectric tensor into a single scalar coefficient.

In the case of a cubic crystal, there will be three independent coefficients in a tensor. According to the notation adopted above, the coefficient μ_{11} is the longitudinal one, μ_{14} is transverse, and μ_{111} is related to shear deformations. Nonzero tensor components can be written down as follows:

$$\mu_{1111} = \mu_{2222} = \mu_{3333} = \mu_{11}, \tag{3}$$

$$\mu_{1122} = \mu_{1133} = \mu_{2121} = \mu_{2233} = \mu_{3131} = \mu_{3232} = \mu_{111}, \tag{4}$$

$$\mu_{1221} = \mu_{1331} = \mu_{2112} = \mu_{2332} = \mu_{3113} = \mu_{3223} = \mu_{14}. \tag{5}$$

The definition allows us to discuss the contributions that could be made by the crystallographic tensor after the rotation process. With regards to a single-axis orientation, the value of the sample frame tensor $\bar{\mu}_{3333}$ is directly correlated to μ_{3333}, thus equaling μ_{11} for out-of-plane longitudinal behavior. With regard to double-axis alignment, the value of the sample frame tensor $\bar{\mu}_{3333}$ is generated as a function of directional cosines, allowing μ_{11}, μ_{14}, and μ_{111} to contribute to longitudinal behavior in the sample frame.

The coefficient ledger on the material image in Figure **??** makes the numeric initialization clear. The DFT collection has a moderately large shear-related value, while the LDA collection has a much more dominant shear value relative to its corresponding longitudinal value. Since the unknown shear term is not known from experiment, the shear value does not act as a rotation input. This image establishes the difference between coefficient scaling and tensor data prior to orientation averaging.

Let μ^c_{pqrs} be the tensor for the flexoelectric effect in the crystallite basis and let R be an appropriate rotation matrix mapping the crystallite frame onto the specimen frame. The rotated tensor is

$$\mu_{ijkl}(R) = R_{ip} R_{jq} R_{kr} R_{ls} \mu^c_{pqrs}. \tag{6}$$

In a polycrystalline material with distribution $\rho(R)$ of orientations R, the orientation-averaged tensor is

$$\bar{\mu}_{ijkl} = \int_{SO(3)} R_{ip} R_{jq} R_{kr} R_{ls} \mu^c_{pqrs} \rho(R)\, dR. \tag{7}$$

The rotation tensor equation forms the essence of the calculation in mathematical form. It excludes a scalar correction of the texture type and forces the transformation of every component of the fourth-rank tensor. Next, the averaging equation transforms the rotations at the grain scale into an overall property. It is homogenization on the texture level but not the

Table 1: Cubic $BaTiO_3$ tensor entries.

Coefficient set	μ_{11}	μ_{14}	μ_{111}
Experiment	5.0×10^4	5.0×10^4	–
DFT	-0.360	1.600	-1.500
LDA	0.150	1.904	-5.460

micromechanical resolution of the local strain gradient field. It thus accounts for the effect of the first order from the statistics of orientations, while stresses at grain boundaries, elastic incompatibilities, size effects of the surface layer, and domain wall motion are left out of account.

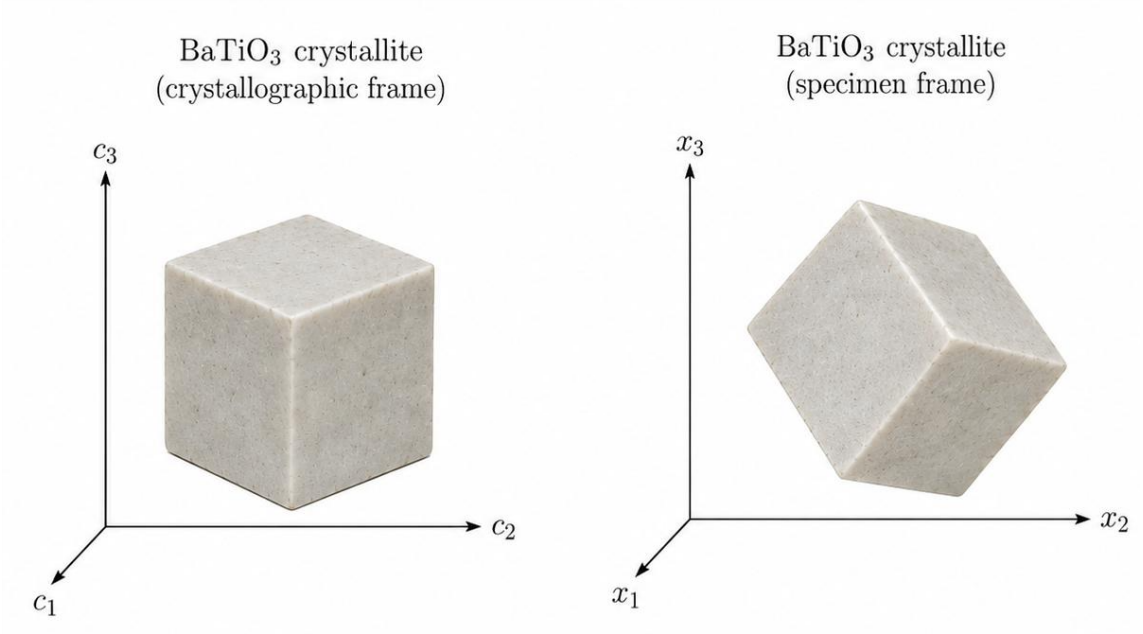

Figure 1: Rotation kernel for the flexoelectric tensor.

In Figure 1, the rotation kernel is highlighted because every tensor index gets transformed. The four components of the effective tensor in specimen coordinates shown below the kernel are the coefficients used in the subsequent steps to establish if the orientation transformation affects just the thickness response or causes redistribution in the whole effective tensor.

Another useful test case is the isotropic limit. For an orientation distribution sampling all the directions evenly on $SO(3)$, the effective tensor becomes isotropic. In the contracted representation, used in the flexoelectric coefficient tensor, the independent isotropic terms satisfy the relation

$$\mu_{111}^{\text{iso}} = \frac{\mu_{11}^{\text{iso}} - \mu_{14}^{\text{iso}}}{2}. \tag{8}$$

This relation is not used in the fitting procedure, but instead serves as a verification test for the isotropy of the average tensor. In particular, the tilt-fiber and isotropic states activate all the rotated tensor indices, yet only the former keeps the directional selectivity of the effective tensor.

4. Coefficients for Cubic $BaTiO_3$, Averaging Orientation

The numerical input parameters are the coefficients of the cubic $BaTiO_3$ flexoelectric tensor provided in Table 1 below. They are given in units of nC/m. Both the DFT and the LDA rows provide all three necessary coefficients to construct the whole cubic tensor according to Eqs. (3)-(5). The experimental row provides only longitudinal and transverse coefficients without the shear coefficient, so the latter cannot be used to rotate the entire tensor. This point is crucial since rotation without the μ_{111} coefficient would destroy the very channel of transfer which we are trying to prove. The published coefficients and the isotropic averaged ones are from a table for the coefficient values of textured polycrystalline dielectrics, see [38].

The information contained in Table 1 consists of two full sets of coefficients and an incomplete experimental reference scale. In the case of the DFT tensor, since it comprises similar magnitudes of coefficients, it can be anticipated that texture will alter the response by some degree. On the other hand, the LDA tensor consists of a very large negative value related to shear as compared to its positive value pertaining to longitudinal, thus altering its response with respect to tilt.

Table 2: Isotropic aggregate reference values.

Coefficient set	μ_{11}^{iso}	μ_{14}^{iso}	μ_{111}^{iso}
DFT	-0.776	1.808	-1.292
LDA	-3.516	3.737	-3.626

Table 2 provides the limits for the isotropic verification and interpretation. Using the DFT set values of $\mu_{11}^{\mathrm{iso}} = -0.776$ nC m^{-1} and $\mu_{14}^{\mathrm{iso}} = 1.808$ nC m^{-1} to calculate with Eq. (8) gives -1.292 nC m^{-1}, which agrees with the isotropic shear-related value in the table. The LDA set returns -3.626 nC m^{-1} using the same two values. Both checks confirm that the random aggregate has achieved the isotropic constraint and further directional design can only be realized by the non-random texture effect.

Tables 1 and 2 provide the numerical information used for the tensor calculations, while Figure **??** shows the sets of coefficients that can be subject to orientation rotation. Hence the orientation average of flexoelectricity calculation starts from the entire DFT and LDA tensor sets instead of one scalar flexoelectric constant. Meanwhile, the experimental row is included for magnitude information comparison purposes but not included for orientation average because there is no shear-related term present.

Four orientations are chosen to differentiate different types of texture effects. In the aligned case, the crystallographic axes are set parallel to those of the specimen and serve as the reference case for the directional single crystal. The zero-tilt fiber orientation aligns the crystallographic [001] direction to the x_3 direction while keeping the in-plane crystallographic axis to randomly oriented within the plane. The tilted-fiber case places the crystallographic axes to a cone with mean tilt of 49.1° while randomizing azimuth and spin angles. Finally, the isotropic case uniformly averages all orientations and stands for the random ceramic sample.

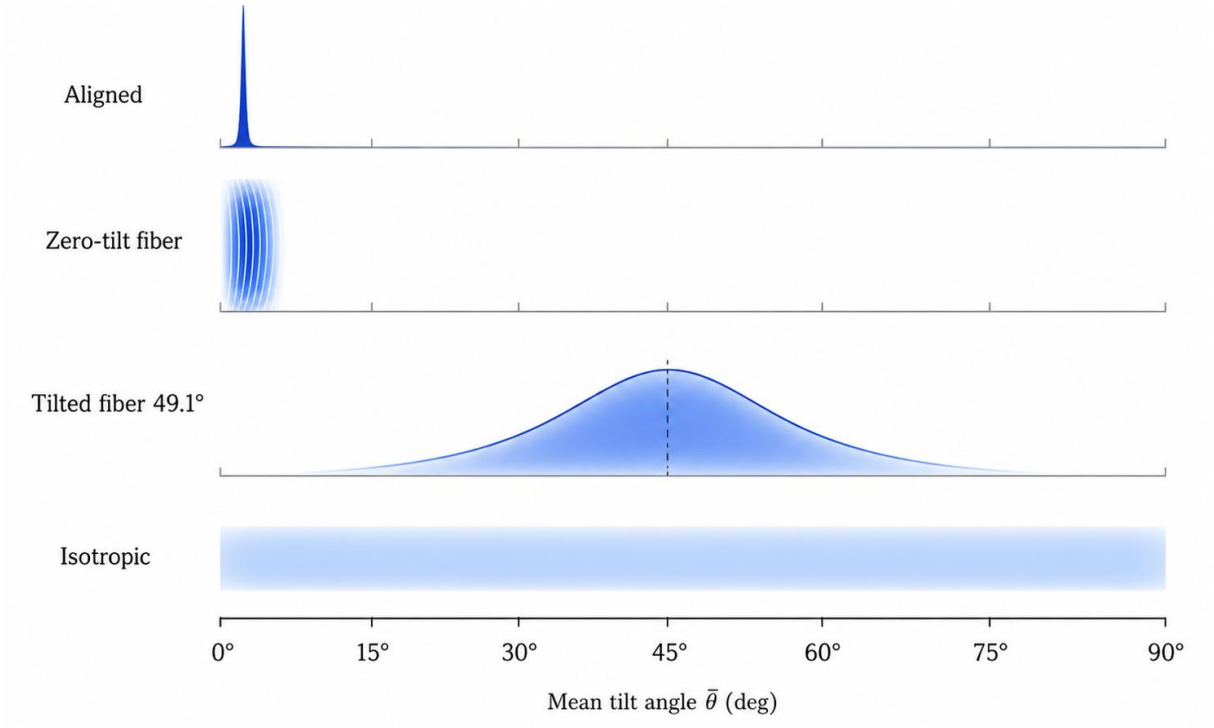

Figure 2: Orientation populations used for averaging.

From the orientations of the populations in Figure 2, we understand that the two fiber textures are different since the former has angular disorder about the thickness axis, whereas the latter does not tilt the crystallographic [001] axis with respect to the thickness axis. It should be emphasized that the tilted-fiber state is essential since only it may couple shear-induced crystallographic behavior to the longitudinal coefficient through rotation.

The finite-width textured material is characterized as follows.

$$\rho_{\eta,\bar{\theta},\sigma}(R) = (1-\eta)\rho_{\mathrm{iso}}(R) + \eta\rho_{\bar{\theta},\sigma}(R), \tag{9}$$

Herein $0 \leq \eta \leq 1$ denotes the texture strength, $\bar{\theta}$ specifies the average tilt angle about the specimen x_3 axis, and σ is the angular deviation. The isotropic distribution has the density $\rho_{\mathrm{iso}} = 1/(8\pi^2)$. In the finite-width textured material, we have

a textured density with uniform sampling of angles,

$$\rho_{\bar{\theta},\sigma}(\psi,\theta,\phi) = \frac{1}{Z(\bar{\theta},\sigma)} \exp\left[-\frac{(\theta-\bar{\theta})^2}{2\sigma^2}\right], \tag{10}$$

where $Z(\bar{\theta},\sigma)$ normalizes the density over $SO(3)$.

The expressions for texture in Eqs. (9) and (10) are probability distributions and not just single orientations. The use of the mixture factor facilitates the inclusion of partial textures, while the use of an angular dispersion ensures that the fiber texture does not become a zero-thickness ring of orientation. The approach is consistent with experimentally measured distributions such as those derived from electron backscattered diffraction, x-ray pole figure analysis, or orientation imaging microscopy since any $\rho(R)$ value can be used within Eq. (7).

The orientation-selection criterion is

$$\mathcal{J}(\eta,\bar{\theta},\sigma) = w_1|\bar{\mu}_{3333}| + w_2|\bar{\mu}_{1331}| - w_3|\bar{\mu}_{1133}| - \lambda \int_{SO(3)} \rho_{\eta,\bar{\theta},\sigma} \ln\left(\frac{\rho_{\eta,\bar{\theta},\sigma}}{\rho_{\text{iso}}}\right) dR. \tag{11}$$

The first term maximizes longitudinal sensitivity at thickness modes, the second one maximizes a possible shear channel allowing transverse-gradient response, and the third minimizes a certain normal-gradient component in the case when cross sensitivity is detrimental. The fourth term corresponds to the relative entropy with respect to the isotropic distribution. The larger the value of λ, the more spread-out orientation distribution is favored, and vice versa.

The objective from Eq. (11) can assign physical significance to the coefficients without implying any universality of their choice. Bending sensors, indenter probes, multilayer capacitors, and porous dielectrics experience different strain-gradient regimes, and the weights should be chosen accordingly. The current calculations focus on the coefficient $\bar{\mu}_{3333}$, since the through-thickness parameter appears to be the most direct target for strain gradients normal to the material surface. However, one can always choose another weight function.

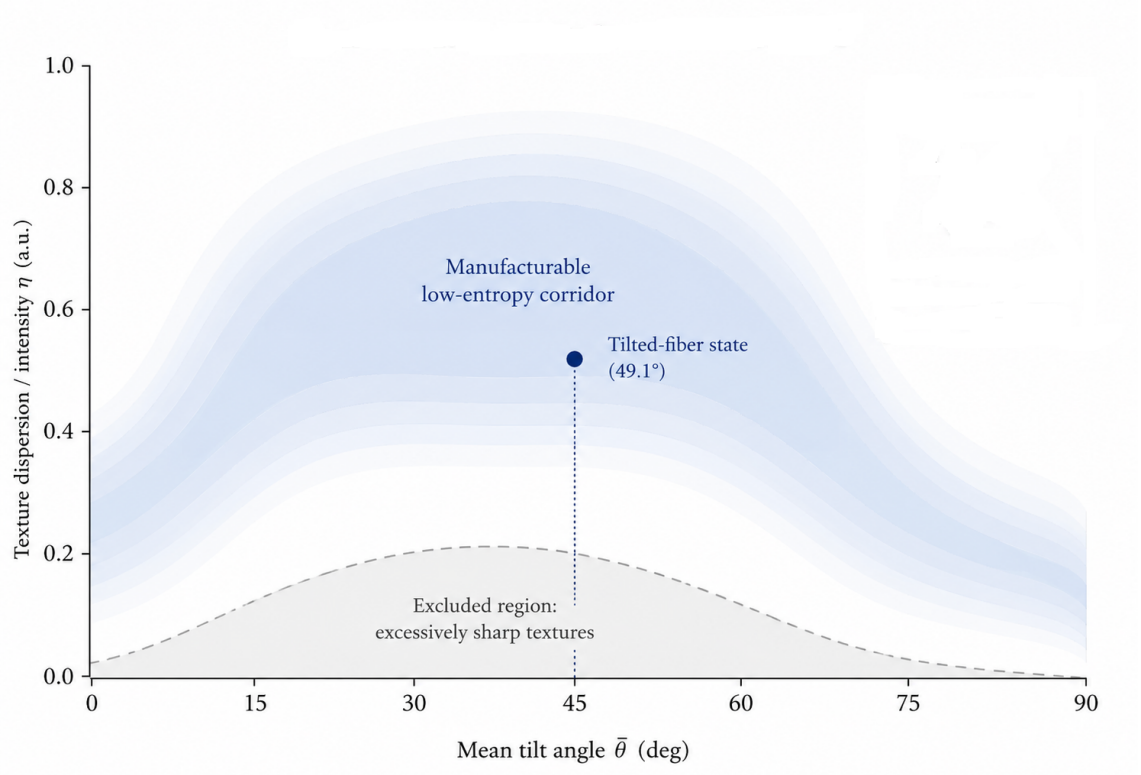

Figure 3: Entropy-limited orientation corridor.

An example of the entropy-constrained orientation corridor of Figure 3 helps to understand the idea of entropy regularization. While the most responsive peak occupies a very narrow band in the orientation space, the chosen state corresponds to a tilted fiber which falls into a wider band that still allows for feasible ceramic processing. Such an observation is highly relevant when designing new materials: a response which is mathematically sharp yet practically inaccessible is of much less value compared to a slightly smaller peak which could be realized by practical processing routes.

The channel transfer shown in Figure 4 forms the link between the orientation model and the results from the simulation. Both DFT and LDA rows employ the same tilted-fiber configuration; however, the hierarchy of the respective coefficients makes the transferred shear coefficient more important in the latter case, thus giving rise to a much lower negative thickness coefficient observed below.

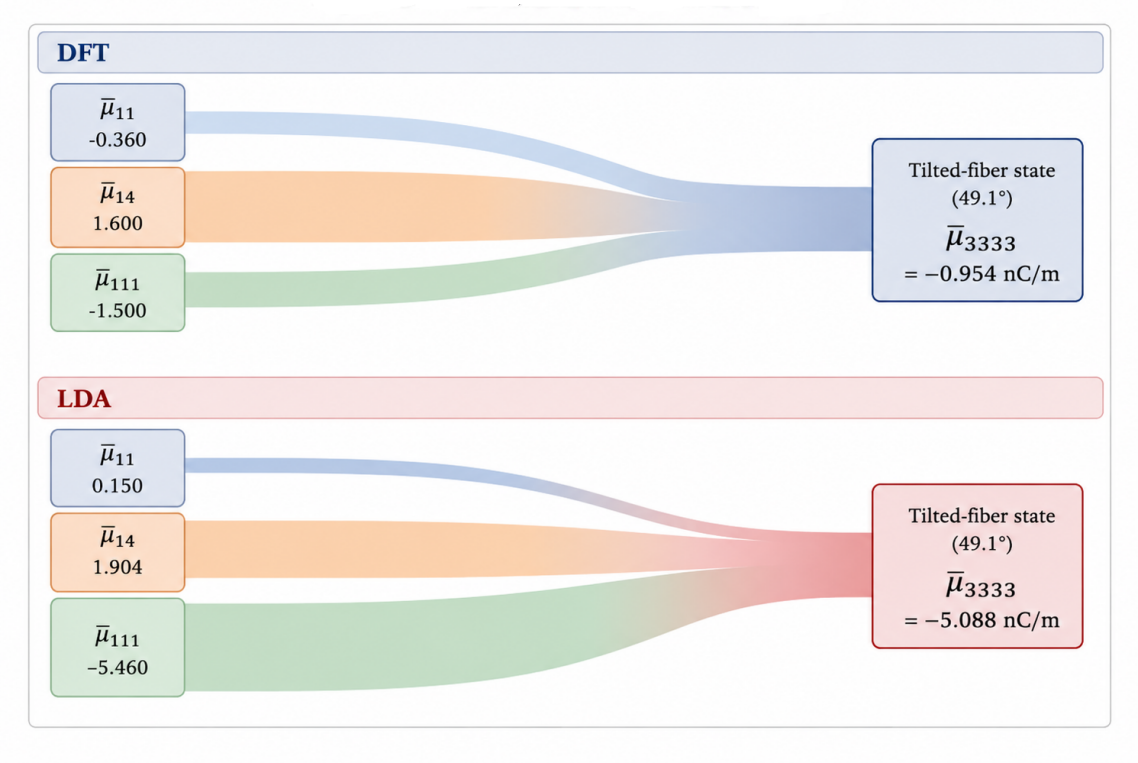

Figure 4: Shear-channel transfer into $\bar{\mu}_{3333}$.

Table 3: Effective flexoelectric coefficients.

Input set	Texture state	$\bar{\mu}_{1111}$	$\bar{\mu}_{1221}$	$\bar{\mu}_{1122}$	$\bar{\mu}_{3333}$
DFT	Aligned	-0.360	1.600	-1.500	-0.360
DFT	Zero-tilt fiber	-0.620	1.860	-1.240	-0.360
DFT	Tilted fiber, 49.1°	-0.843	1.786	-1.314	-0.954
DFT	Isotropic	-0.776	1.808	-1.292	-0.776
LDA	Aligned	0.150	1.904	-5.460	0.150
LDA	Zero-tilt fiber	-2.141	4.196	-3.168	0.150
LDA	Tilted fiber, 49.1°	-4.106	3.541	-3.823	-5.088
LDA	Isotropic	-3.516	3.737	-3.626	-3.516

5. Results and discussion

5.1 Effective coefficients in different orientation states

The calculated effective coefficients in each orientation state are presented in Table 3. The complete fourth-order notation is chosen intentionally since it reflects that there are not several constants, but only one single rotated and averaged tensor. Such representation also demonstrates how the transfer takes place as the same crystalline coefficient may take a different position relative to the specimen frame depending on the texture.

The data in Table 3 reveal three regimes of responses. The aligned regime is only responsible for providing the crystallographic data in the respective directions. The regime for zero-tilt fiber causes a modification of the in-plane data due to spin around the thickness direction that redistributes the tensor components in the transverse plane; however, no change occurs in $\bar{\mu}_{3333}$ since the crystallographic direction [001] continues to be parallel to x_3. The tilted-fiber regime modifies the projection and provides the highest magnitude of thickness mode for both sets of coefficients. The isotropic regime activates additional channels by orientation averaging but at the expense of directional sensitivity and thus yields lower $|\bar{\mu}_{3333}|$ compared to the tilted-fiber regime.

The signatures of Figure 5 should be interpreted as channel-transfer maps. For the DFT set, the variation in the change of responses is relatively mild due to similar magnitude longitudinal, transverse, and shear-related tensor components. The tilted-fiber row is different, however: the coefficient $\bar{\mu}_{3333}$ attains -0.954 nC m^{-1} for the tilted fibers, while the perfectly aligned and randomly oriented specimens stay at -0.360 nC m^{-1}. For the LDA set, the contrast between the longitudinal and shear-related terms is higher, and thus, the tilted-fiber response $\bar{\mu}_{3333} = -5.088$ nC m^{-1} includes an especially large negative component.

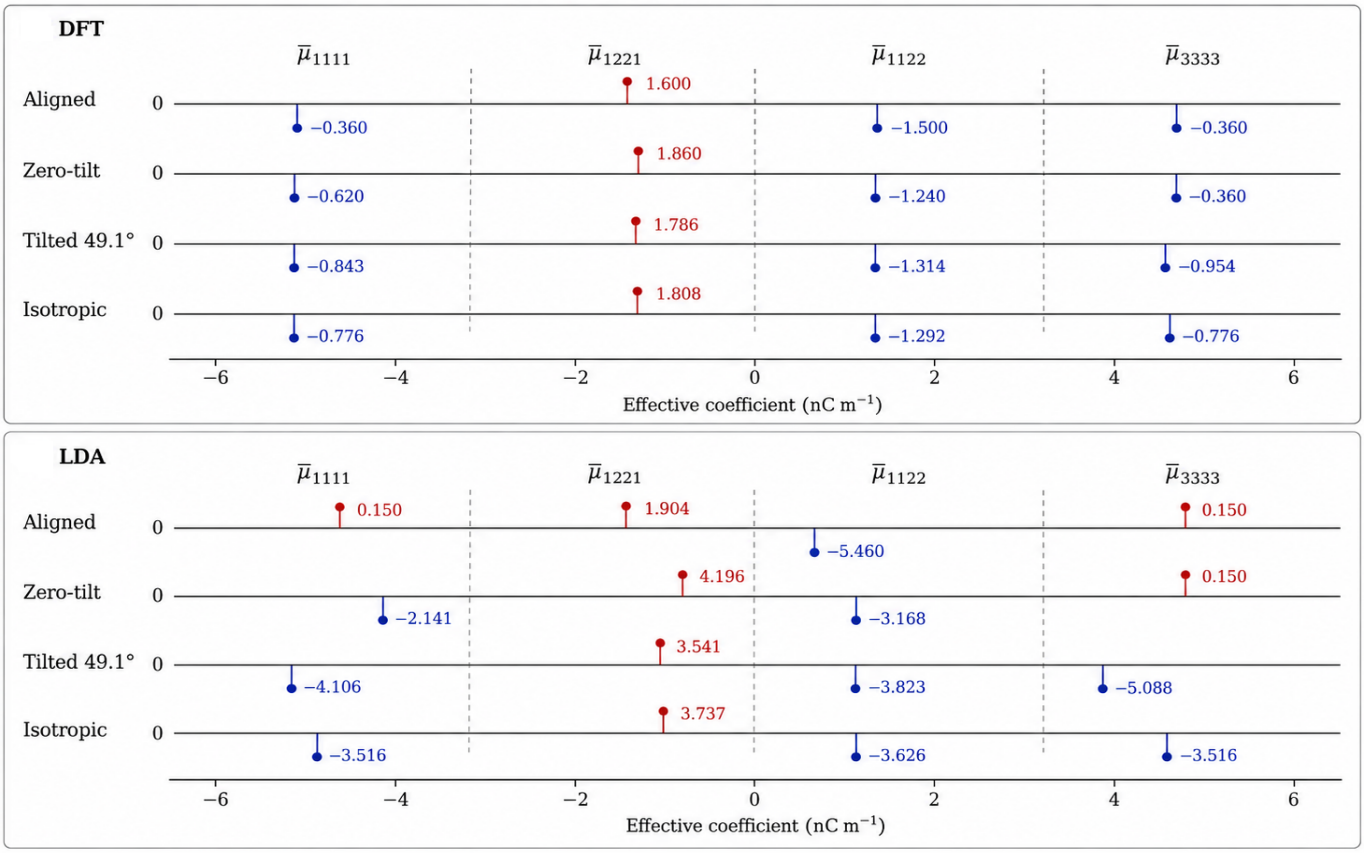

Figure 5: Signed fingerprints of effective tensor components.

From the DFT calculations, one sees that control of the degree of tilt may lead to better performance than perfect alignment or randomization even if the coefficient hierarchy is not very sharp. Perfectly aligned specimen gives $\bar{\mu}_{3333} = -0.360$ nC m^{-1}. No tilt does not affect the response since spin randomization along the fiber axis cannot change the coefficient. The value of isotropic distribution is -0.776 nC m^{-1} and greater in magnitude than the previous one due to activation of other channels by rotational averaging. However, the greatest value is reached with the tilting procedure at -0.954 nC m^{-1}. This way, a directional texture proves to be preferable to full randomization for certain specimens' tensor coefficients.

The LDA example demonstrates a more spectacular phenomenon. Here, the aligned thickness coefficient takes the value 0.150 nC m^{-1}, which is the positive longitudinal term of 0.150 nC m^{-1}. The zero-tilt fiber row leaves this value unchanged. In contrast, the tilted-fiber row provides $\bar{\mu}_{3333} = -5.088$ nC m^{-1} because now the shear-related coefficient is involved. The value of isotropic distribution is -3.516 nC m^{-1} since averaging involves all available coefficients. Hence, it is seen that the choice of tilt allows the use of this particular negative contribution much more efficiently for the out-of-plane direction.

5.2 Thickness-mode gain and polarity

The thickness-mode case analysis is confined to Table 4. Diagnostic ratios include two types. First, the aligned gain G_{3333} measures each texture against perfect alignment, whereas the isotropic gain A_{3333} measures each texture against the random aggregate. These gain values are not extra material parameters but interpretive measures for assessing whether the texture state enhances the target parameter with respect to some reference level.

Table 4 indicates the primary outcome of the analysis by the values of these indices. The tilted-fiber texture exhibits superiority not only to the perfectly aligned one but also to the isotropic aggregate, regardless of which full set of coefficients is considered. For the case of DFT, the corresponding gains are 2.65 and 1.23, respectively, while in the case of LDA, they are 33.92 and 1.45. On the other hand, the zero-tilt fiber state provides no improvement in the thickness parameter despite its effects on other tensors' coefficients. Thus, it is clear that what matters is not the presence of fiber texture per se, but rather the crystallographic angle tilt relative to the specimen thickness.

The signed comparison of thickness for Figure 6 brings up a device-level complication that is not apparent in the whole map of coefficients. In the case of the DFT series, the tilted texture boosts the magnitude but preserves the negativity of the thickness coefficient. On the other hand, the tilted texture in the LDA series modifies both the magnitude and the sign. Hence, designing a sensor based on the LDA series of coefficients is complicated. A texture which increases sensitivity can

Table 4: Thickness-response indices.

Input set	Texture state	$\lvert\bar{\mu}_{3333}\rvert$	G_{3333}	A_{3333}
DFT	Aligned	0.360	1.00	0.46
DFT	Zero-tilt fiber	0.360	1.00	0.46
DFT	Tilted fiber, 49.1°	0.954	2.65	1.23
DFT	Isotropic	0.776	2.16	1.00
LDA	Aligned	0.150	1.00	0.04
LDA	Zero-tilt fiber	0.150	1.00	0.04
LDA	Tilted fiber, 49.1°	5.088	33.92	1.45
LDA	Isotropic	3.516	23.44	1.00

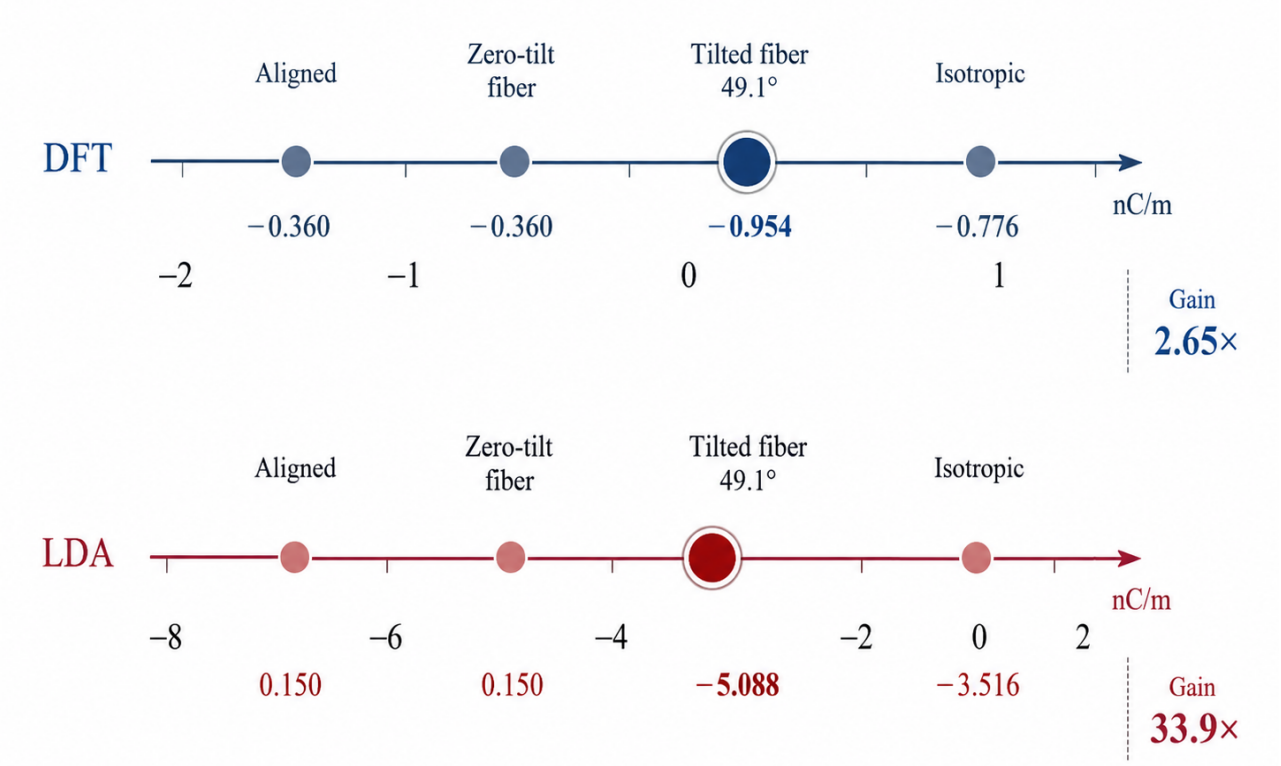

Figure 6: Thickness coefficient under four textures.

also change the sign of the induced charge when subjected to nominally similar strain gradients.

This property will be an asset, rather than a drawback, if properly recognized in the initial design of the sensing system. For example, the polarity of output from the bending sensor is determined by the arrangement of electrodes as well as by the sign convention adopted for the strain gradient and the sign of the effective coefficient of piezoelectricity. A texture which causes the response to switch from positive aligned $\bar{\mu}_{3333}$ to negative tilted $\bar{\mu}_{3333}$ will imply a different polarity compared to an aligned sample. The same sign problem may arise in multilayers, where it will control their constructive or partial destructive interaction. Texture design therefore affects both amplitude and phase of the electromechanical response.

5.3 Zero-tilt fiber as a control state

This texture is not a failed texture; rather, it is a control texture which highlights the importance of angular projection. Since the crystallographic [001] axis maintains its alignment relative to x_3, the thickness tensor still samples the same channel of the aligned state. Thus, $\bar{\mu}_{3333}$ remains -0.360 nC m^{-1} for the DFT set and 0.150 nC m^{-1} for the LDA set. The spin disorder about the thickness axis does not affect the projection of [001].

Spin disorder in the same texture has an even stronger effect on planar tensors. In particular, for the LDA set, $\bar{\mu}_{1111}$ changes from 0.150 to -2.141 nC m^{-1}, while $\bar{\mu}_{1221}$ rises from 1.904 to 4.196 nC m^{-1}. In the DFT set, the changes are similar. $\bar{\mu}_{1111}$ goes from -0.360 to -0.620 nC m^{-1}, and $\bar{\mu}_{1221}$ increases from 1.600 to 1.860 nC m^{-1}. It seems that although spin disorder degrades the [001] fiber texture, it can still have a positive impact on other types of strain-gradient field components (particularly, lateral and radial strain). Hence, one cannot consider a strong ceramic process as a successful process based solely on the fact that it yields a strong [001] fiber texture without considering the strain-gradient field distribution in a particular device.

The importance of this interpretation lies in the reporting of experimental results. While the pole figure or orientation map might show an evident fiber texture, it is important to report the distribution of tilt angle and the tensor component as well. Fiber texture with zero tilt and with a non-zero tilt are both well-ordered structures, but their respective crystallographic axes projected into the $\bar{\mu}_{3333}$ differ from each other. The results, therefore, support the need for reporting textures in conjunction with the tensor components predicted. In the case of flexoelectrics, the issue is not about the presence of texture in ceramics; rather, it is about whether the correct tensor component is aligned with the strain gradient.

5.4 Mechanism behind tilted fiber amplification

Tilted fiber amplification originates from the rotation in Eq. (6). Grains that tilt away from the specimen normal direction contribute not just the crystallographic longitudinal channel, but a mixture of the three components in Eq. (**??**), and the amount of the shear-related contribution dominates the averaged coefficient $\bar{\mu}_{3333}$ for the tilted fiber.

Shear channel amplification illustrated in Figure 4 must not be confused with a simple magnification of tensor coefficients. The material is still $BaTiO_3$ with the same crystallite coefficients; the gain comes purely from a change in the specimen frame. From the perspective of materials design, the process is significant because it implies a path to achieving a desired tensor channel without changing the crystal composition. Instead of searching for an appropriate substitution, one would merely have to project an existing crystallographic coefficient in a particular direction.

Comparing the DFT and LDA coefficient sets, we see that the tilted-fiber mechanism works identically for both systems, although it yields a much stronger effect in the latter due to the different coefficient hierarchy. The DFT coefficients exhibit a moderate gain, which occurs since the shear-related and transverse components are comparable to the longitudinal coefficient. In the case of the LDA model, the shear channel $-\mu_{111} = 5.460$ nC/m gives a much greater value than $\mu_{11} = 0.150$ nC/m, and the tilting produces a very strong amplification.

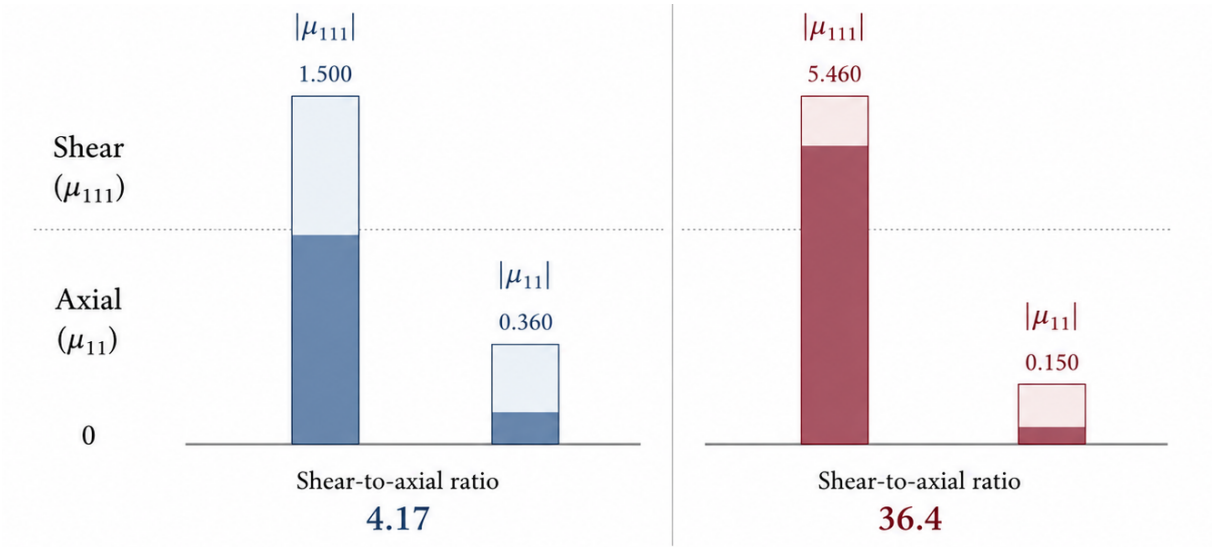

Figure 7: Shear dominance controls amplification.

The relationship between the hierarchy and response gain is demonstrated in Figure 7: The DFT shear-to-longitudinal ratio is 4.17 and results in the 2.65 times gain for $\bar{\mu}_{3333}$. For the LDA set with the ratio of 36.4, the gain reaches 33.9. This result confirms that the amplifying orientation process yields a much stronger response for a crystal with a larger shear-related component compared to the longitudinal coefficient.

From the practical perspective, the tilted fiber effect can be considered a trade-off between channel purity and access. The fully aligned system has optimal tensor order, but it activates the least desirable tensor component. Fully randomized grains provide maximum access to all the tensor entries but destroy any directional preference. The tilted fibers allow sampling of the strongest shearing component while maintaining directional response along the specimen thickness. This explains why the tilted state exceeds isotropy in both coefficient sets even though isotropy also activates additional tensor components.

5.5 Comparison with the isotropic ceramic limit

Isotropic aggregates are not only a theoretical limit case; rather, they show what the outcome would be in case the texture information was fully randomized. For DFT, the corresponding thickness coefficient is -0.776 nC m^{-1}; this number is greater in absolute value than in the case of aligned samples, yet smaller than in tilted-fibers. For LDA, the isotropic thickness

coefficient is -3.516 nC m^{-1}; this time, too, it is larger in absolute value than in the perfectly-aligned sample, but smaller than in tilted-fibers. As seen from this pattern, randomization helps unlock hidden tensor channels, but directed texture prevails once a specific specimen orientation is needed.

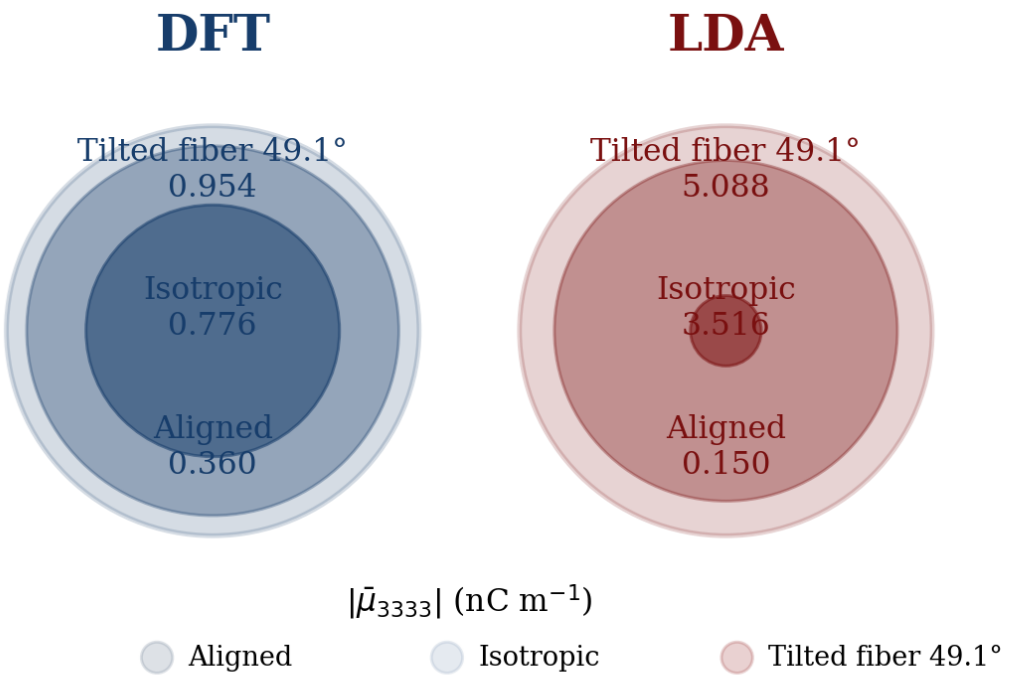

Figure 8: Tilted texture exceeds the isotropic limit.

A comparison by radius ranges, presented in Figure 8, demonstrates the same point irrespective of any signs. For each coefficient series, we observe an enclosure relation: the value of tilted-fibers encloses the value of isotropy, and that encloses the value of perfectly-aligned samples. This proves that orientation disorder itself helps raise the thickness coefficient, yet a tilt retains enough directional selectivity to surpass the random aggregate.

Another benefit of isotropic state is that it helps avoid misinterpreting results when analyzing "random ceramics". Indeed, one observes from the LDA coefficient values that random orientation produces a significantly larger thickness coefficient than perfect alignment since the isotropic aggregate taps into the powerful shear-related channel. One should bear in mind this effect during computations in order not to mistakenly underestimate the potential response of a polycrystalline material. In particular, a small coefficient value obtained for aligned specimens does not mean that polycrystals will respond less effectively since an increased orientation disorder will allow more tensor contributions. The drawback of the isotropic aggregate, of course, is its inability to distinguish between different specimen orientations.

In turn, the results provide hints about what texture coefficients should be taken into account when selecting suitable processes for computational screening. Although in case of isotropic aggregate, Eq. (7) predicts a significant response due to redistribution of cubic tensor anisotropy, once a process produces a non-zero tilt, the result will likely exceed the isotropic value. It is therefore necessary, when conducting calculations, to compare possible textures with two reference limits – aligned and isotropic, respectively.

5.6 Processing implications

The results indicate a straightforward processing-to-functionality criterion: texture orientation should follow the tensor channel associated with the strain gradient direction. In a bending sensor based on a thickness mode, the key component is $\bar{\mu}_{3333}$, provided the principal strain gradient is through the thickness. In case of a material indented by a probe, the loading environment would involve localized shear and/or normal gradients. Multilayer dielectrics and coatings experience localized gradients parallel to layer interfaces, while porous ceramics develop a significant local curvature and gradient field around the pores. Orientation distributions suitable for each application would differ.

This loading map in Figure 9 illustrates a link between the tensor components to the environments characterized by strain gradients. Bending through the thickness and indentation would be consistent with the tilted fiber condition due to the opportunity to utilize the reoriented shear channel in both cases. Interfaces within a layered system would allow the zero-tilt or aligned conditions for processing if the gradients occur perpendicularly to the interface plane. The porosity and

Figure 9: Texture choice as dictated by strain-gradient loading environments.

curvature would be consistent with the random condition as the gradients tend to vary in the neighborhood of pores and/or curved sections. Therefore, the figure depicts possible orientation distributions relative to specific device geometries, but it does not necessarily imply a unique processing approach for obtaining the required textures.

The ceramic processing methods may be analyzed within this framework. Template grain growth may create texture by using anisotropic templates during processing. Tape casting and other thin film manufacturing techniques may create anisotropic grain orientation and packing. Constrained sintering and hot forging may create a texture by influencing crystalline structure formation. Field assisted sintering may impact texture development through the sintering process itself via densification, grain boundary migration, or thermal gradients. These processing techniques have different capabilities for controlling tilt angle, intensity, and angular spread of the texture. Entropy regularization introduces specific measurable processing factors, which include intensity parameter η, mean tilt $\bar{\theta}$, and angular spread σ.

The importance of LDA results for processing decisions cannot be overstated. In case of the dominant shear-related coefficient, a technique solely focused on maximizing axial alignment of grains can turn out to be counterproductive as a thickness mode sensor. A well-controlled tilt close to the preferred cone angle would yield a higher value of this tensor channel component. It does not mean, however, that every $BaTiO_3$ ceramic has to be oriented at 49.1°. Rather, the optimum value depends on tensor hierarchy and the desired device behavior. A particular angle has been used in order to highlight the nature of the transfer mechanism. All measured and simulated textures have to be evaluated against a complete tensor to determine their functional significance.

If only the longitudinal component in the crystallographic coordinate system were to be considered, the aligned texture would clearly be a more natural choice and the LDA tensor orientation state would be unsuitable for a thickness mode sensor since μ_{11} is only 0.150 nC/m[1]. The present work suggests that this expectation needs to be revised. A dominant shear-related coefficient exists in the LDA orientation state and a geometric reorientation of the corresponding tensor channel is achieved thanks to the tilted fibers. This explains how a component that is shear-related in crystallographic coordinates controls a longitudinally related tensor channel. As demonstrated by the example, it is a nontrivial decision that affects processing choice because the two orientation states would receive fundamentally different evaluations under the scalar selection scheme.

Another way to interpret this finding is to evaluate potential design risks associated with a chosen processing path. The ceramic path designed solely to maximize texture sharpness may end up focusing on creating visually striking textures that may fail to exhibit desired functional characteristics. On the other hand, the technique that focuses on tilting while allowing

angular spread around the preferred angle can produce higher values for the coefficient of interest. This is consistent with the idea of penalizing the designs that are too sharply aligned and favor those with sufficient angular spread to be reasonable. For functional ceramics, the correct design principle would therefore be to maximize usable tensor projection.

5.7 Significance of material design

From a materials-design perspective, the significance is that the shear flexoelectric coefficient cannot be thought of as a correction term. If one considers only a single-axis flexoelectric tensor, with a scalar point of view towards flexoelectric properties, then the longitudinal coefficient would appear to be a better place to consider through-thickness behavior. However, the rotation in the tensor shows that the assumption can go wrong even with the simple tilt of crystallographic axes. There exists a scenario where a shear coefficient contributes significantly to the longitudinal component of a response in the specimen frame. This conclusion is particularly evident with the LDA coefficient tensor where aligned thickness response is negligible but a large and negative tilting response appears.

Additionally, a more general principle follows from the formulation for anisotropic functional materials: tensorial structures of properties must correspond to strain gradient fields in order to optimize performance. The rule is well known in elasticity and plasticity. Yet, in some way, it can be somewhat underestimated in discussion of flexoelectric ceramics when only effective scalar coefficients are reported in experiments. Such a scalar coefficient is appropriate for the comparison between two specimens of a given geometry, but it fails to guide the design of textures in the strain gradient field environment.

From a methodology perspective, the calculation is sufficiently compact for screening but preserves all physics associated with tensorial properties. No extensive finite element models with microstructures are required for the evaluation of every texture. The screening allows ranking of the textures before costly numerical analysis is performed. Only promising orientation distributions have to be investigated in a detailed analysis that includes elastic anisotropy, boundary conditions at grain boundaries, finite-size effects, electrode geometry and field concentrators. The average over orientations thus acts as a prescreening tool.

5.8 Implications for interpreting measured coefficients

Bulk flexoelectric measurements on ceramics are plagued by high variability because they may include intrinsic response, amplified dielectric contributions, surface piezoelectricity, residual stress fields, defect gradients, phase heterogeneity, and testing boundary conditions [8]. Review evidence also shows that nanoscale and surface-sensitive contributions can enter the measured response [6]. Flexoelectric studies of complex domains further indicate that boundary and microstructural conditions may influence effective coefficients [39]. Computational studies likewise show that microstructure and geometry can modify the apparent response [35]. Here we further expand that list of possibilities by adding texture as an interpretive variable. Ceramics of the same chemical composition and comparable density might possess different effective coefficients depending on whether their texture projects their tensorial channels favorably or not. Moreover, the appearance of a strong response does not necessarily mean larger values of the corresponding intrinsic tensor components; rather, this could imply more favorable textures of orientation distribution.

Such distinctions are important when performing comparisons between experimental data and calculations based on first-principles approaches. First-principles work provides information about intrinsic tensor components for crystals under well-defined boundary conditions [14]. Modern theory clarifies how bulk and surface contributions must be separated when interpreting finite specimens [16]. Experimental and theoretical analysis of flexoelectric response in ferroelectric systems also shows that measured values may combine several mechanisms [40]. Orientation averaging provides one possible means of bridging the gap between these two different regimes. While orientation averaging is far from being a silver bullet, its use is crucial for avoiding erroneous conclusions about intrinsic behavior by comparing a coefficient reported for the specimen frame with a crystallographic component.

Consequently, a useful experimental technique should consist of two parts. One part includes electromechanical measurements, whereas the other includes determination of the orientation distributions through electron backscattered diffraction or X-ray pole figure analysis. Such a measurement technique will provide the necessary inputs for predicting the tensor projection effects using Eq. (7). Any deviation from this expected response then implies additional physics at play. In this way, texture-aware modeling improves not only design but also diagnosis.

5.9 Multiple tensor channels and design trade-offs

Four remaining tensor coefficients imply that design for a single material output is not possible. A texture capable of boosting $\bar{\mu}_{3333}$ will alter $\bar{\mu}_{1111}$, $\bar{\mu}_{1221}$, and $\bar{\mu}_{1122}$ in unpredictable directions. For the DFT material, the change in $\bar{\mu}_{1111}$ between the aligned and the tilted fiber states goes from -0.360 to -0.843 nC m^{-1} while $\bar{\mu}_{1221}$ remains close to its isotropic

level. Similarly, for the LDA material, the change is from -5.490 nC m^{-1} to -4.106 nC m^{-1} for $\bar{\mu}_{1111}$ and from -0.514 to 3.541 nC m^{-1} for $\bar{\mu}_{1221}$. The numbers demonstrate that, rather than amplifying a certain tensor coefficient, texture reorganizes its content across several specimen-frame channels. Thus, a thickness gradient sensor with low lateral cross-sensitivity must be designed based on a more extensive criterion than $\bar{\mu}_{3333}$ alone.

The behavior of the $\bar{\mu}_{1122}$ is of special interest in evaluating cross coupling between normal and thickness modes. With a DFT material, this coefficient changes from -1.500 nC m^{-1} for an aligned fiber to -1.314 nC m^{-1} for a tilted texture. Since $\bar{\mu}_{1122}$ is relatively small, its change is modest because DFT does not possess a strongly dominant shear channel. For LDA, the values are -5.460 nC m^{-1} and -3.823 nC m^{-1}, respectively. Here, the thickness response becomes larger, while the selected cross-normal coefficient is smaller compared to the aligned value. This result shows the possibility of enhancing thickness responses without maximizing other responses that could give rise to undesirable lateral cross-sensitivity. This characteristic can be exploited by increasing the penalty weight on such a cross-coupled coefficient in the entropy regularized objective defined in Eq. (11).

The behavior of $\bar{\mu}_{1221}$ as opposed to $\bar{\mu}_{3333}$ helps distinguish access to a shear-related crystallographic tensor coefficient from transfer of its response into thickness mode. The aligned zero-tilt fiber state yields the largest value of $\bar{\mu}_{1221}$ of 4.196 nC m^{-1}, which does not affect $\bar{\mu}_{3333}$. The conclusion is that, while a certain specimen frame channel with a high shear coefficient can be activated with the help of a proper distribution, this activation does not necessarily convert its contribution to the desired thickness mode. The correct distribution transfers the selected channel tensor product to the 3333 combination. The tilted texture is, therefore, a shear-rearranged texture for the purpose of converting shear response into thickness mode.

These examples highlight the utility of multiple tensor channel representation for sensor design. High sensitivity to strain gradient requires a dominant tensor coefficient, which, however, may not be sufficient. Large secondary channels may lead to response to undesired lateral gradients, asymmetric mounting, or mechanical shear arising from external contact. In addition, different electrodes, sensing element geometries, and array layouts may favor detection of certain tensor components more than others. Therefore, the designer can choose to emphasize either $\bar{\mu}_{3333}$ in Eq. (11) or penalize certain tensor coefficients that produce cross coupling in terms of a certain sensing geometry and strain gradient directionality. The goal is no longer to optimize a single output coefficient, but to control several tensor channels in parallel.

In addition, the design choices can include selection of appropriate electrode pattern and geometry. An electrode layout that detects out-of-plane response favors $\bar{\mu}_{3333}$ coefficient. On the other hand, interdigitated electrodes may detect both thickness and lateral normal components. A microbeams under bending, membranes with surface indentation, and coatings on curved surfaces can sample several tensor coefficients at once. Hence, it becomes obvious that the optimal texture cannot be selected independent of the mechanical field and measurement geometry. Texture selection, electrode layout, and strain gradient field become an inseparable optimization problem.

Finally, the observation about the LDA sign change illustrates the necessity of using tensor fingerprints rather than scalar representations. In practice, when measuring the total charge response, the effect of the change would be simply interpreted as increased signal amplitude. However, in addition to the amplitude, the sign difference reveals the change in the direction of the effective polarization induced by texture modification. When assembling arrays and layers, such directional information becomes crucial for ensuring that outputs add up or produce spatially varying signals. Therefore, the design protocol must include recording of the signs of effective tensor coefficients, not merely their absolute values.

Overall, the preceding discussion reinforces the importance of signed tensor fingerprints beyond visual representation. They serve not only as a summary, but as a means of identifying texture effect on selectivity of tensor amplification. For DFT material, the fingerprint plot set shows relatively low texture impact on tensor rearrangement, with a minor increase in the thickness response channel. For LDA, the fingerprints indicate strong re-orientation of tensor, dominated by the transfer of a highly negative value from the shear channel. The two sets can be considered indicative of distinct material design approaches.

6. Conclusions

The calculations show whether a finite-width tilted-fiber texture can beat the performance limit in perfectly aligned and isotropic aggregates by exploiting crystallographic response associated with shear through its transformation into the thickness component of the tensor in specimen frame. The answer to both cases under consideration is positive. The DFT tensor exhibits only moderate improvement: $\bar{\mu}_{3333}$ rises from 0.360 nC m^{-1} in aligned state to 0.954 nC m^{-1} in the tilted-fiber case, which corresponds to a factor of 2.65 improvement compared to aligned texture and a 23% advantage over the isotropic aggregate. In the case of the LDA tensor, however, the improvement is very strong: $\bar{\mu}_{3333}$ grows from 0.150 nC m^{-1} to -5.088 nC m^{-1}, which corresponds to a 33.9-fold enhancement over alignment and a 45% benefit over the isotropic aggregate.

The reason behind is tensor-channel transfer. The random texture at zero tilt randomizes the spin along the thickness axis and affects the in-plane components, but does not affect the thickness coefficient since the crystallographic [001] direction still runs along the x_3 axis. The tilted-fiber texture changes the projection geometry and enables a contribution of shear-related or transverse crystallographic entries to the nominally longitudinal component in specimen frame. Transfer is expected to be moderate if all the four coefficients in question are of comparable magnitudes and pronounced in case when the largest of them is shear-related.

The general design principle emerging from these results is as follows. Optimal flexoelectric texture cannot be achieved by maximal alignment alone. If the largest flexoelectric coefficient is shear-related, some tilting of fibers is required to achieve the best possible response along the nominal axis. It would be beneficial to maximize the degree of texture dispersion and minimize the number of preferred orientations to make it processing-friendly via entropy regularization. As a result, for a material like textured $BaTiO_3$ ceramics, the optimal texture is one that projects the strongest tensor channel in the relevant loading direction.

References

[1] Kogan, S. M. (1964). Piezoelectric effect during inhomogeneous deformation and acoustic scattering of carriers in crystals. Sov. Phys. Solid State, 5(10), 2069-2070.
[2] Mindlin, R. D. (1963). Microstructure in linear elasticity (No. TR50).
[3] Mindlin, R. D. (1968). Polarization gradient in elastic dielectrics. International Journal of Solids and Structures, 4(6), 637-642.
[4] Tagantsev, A. K. (1986). Piezoelectricity and flexoelectricity in crystalline dielectrics. Physical Review B, 34(8), 5883.
[5] Tagantsev, A. K. (1991). Electric polarization in crystals and its response to thermal and elastic perturbations. Phase Transitions: A Multinational Journal, 35(3-4), 119-203.
[6] Zubko, P., Catalan, G., & Tagantsev, A. K. (2013). Flexoelectric effect in solids. Annual Review of Materials Research, 43(1), 387-421.
[7] Nguyen, T. D., Mao, S., Yeh, Y. W., Purohit, P. K., & McAlpine, M. C. (2013). Nanoscale flexoelectricity. Advanced Materials, 25(7), 946-974.
[8] Yudin, P. V., & Tagantsev, A. K. (2013). Fundamentals of flexoelectricity in solids. Nanotechnology, 24(43), 432001.
[9] Wang, B., Gu, Y., Zhang, S., & Chen, L. Q. (2019). Flexoelectricity in solids: Progress, challenges, and perspectives. Progress in Materials Science, 106, 100570.
[10] Shu, L., Wei, X., Pang, T., Yao, X., & Wang, C. (2011). Symmetry of flexoelectric coefficients in crystalline medium. Journal of Applied Physics, 110(10).
[11] Ma, W., & Cross, L. E. (2006). Flexoelectricity of barium titanate. Applied Physics Letters, 88(23).
[12] Cross, L. E. (2006). Flexoelectric effects: Charge separation in insulating solids subjected to elastic strain gradients. Journal of materials science, 41(1), 53-63.
[13] Maranganti, R., & Sharma, P. (2009). Atomistic determination of flexoelectric properties of crystalline dielectrics. Physical Review B—Condensed Matter and Materials Physics, 80(5), 054109.
[14] Hong, J., & Vanderbilt, D. (2011). First-principles theory of frozen-ion flexoelectricity. Physical Review B—Condensed Matter and Materials Physics, 84(18), 180101.
[15] Tagantsev, A. K., & Yurkov, A. S. (2012). Flexoelectric effect in finite samples. Journal of Applied Physics, 112(4).
[16] Stengel, M. (2013). Flexoelectricity from density-functional perturbation theory. Physical Review B—Condensed Matter and Materials Physics, 88(17), 174106.
[17] Nye, J. F. (1985). Physical properties of crystals: their representation by tensors and matrices. Oxford university press.
[18] Bunge, H. J. (2013). Texture analysis in materials science: mathematical methods. Elsevier.
[19] Roe, R. J. (1965). Description of crystallite orientation in polycrystalline materials. III. General solution to pole figure inversion. Journal of Applied Physics, 36(6), 2024-2031.
[20] Kocks, U. F., Tomé, C. N., & Wenk, H. R. (2000). Texture and anisotropy: preferred orientations in polycrystals and their effect on materials properties. Cambridge university press.
[21] Beran, M. J., & Pytte, A. (1968). Statistical continuum theories. American Journal of Physics, 36(10), 923-923.
[22] Hill, R. (1965). A self-consistent mechanics of composite materials. Journal of the Mechanics and Physics of Solids, 13(4), 213-222.
[23] Mura, T. (2013). Micromechanics of defects in solids. Springer Science & Business Media.
[24] Torquato, S. (2002). Random heterogeneous materials: microstructure and macroscopic properties (Vol. 16). New York: Springer.
[25] Jaynes, E. T. (1957). Information theory and statistical mechanics. Physical review, 106(4), 620.
[26] Kullback, S., & Leibler, R. A. (1951). On information and sufficiency. The annals of mathematical statistics, 22(1), 79-86.
[27] Cover, T. M. (1999). Elements of information theory. John Wiley & Sons.
[28] Varadhan, S. S. (1984). Large deviations and applications. Society for Industrial and Applied Mathematics.
[29] Ma, W., & Cross, L. E. (2001). Large flexoelectric polarization in ceramic lead magnesium niobate. Applied Physics Letters, 79(26), 4420-4422.
[30] Ma, W., & Cross, L. E. (2002). Flexoelectric polarization of barium strontium titanate in the paraelectric state. Applied Physics Letters, 81(18), 3440-3442.
[31] Eliseev, E. A., Morozovska, A. N., Glinchuk, M. D., & Blinc, R. (2009). Spontaneous flexoelectric/flexomagnetic effect in nanoferroics. Physical Review B—Condensed Matter and Materials Physics, 79(16), 165433.
[32] Hong, J., & Vanderbilt, D. (2013). First-principles theory and calculation of flexoelectricity. Physical Review B—Condensed Matter and Materials Physics, 88(17), 174107.
[33] Stengel, M. (2014). Surface control of flexoelectricity. Physical Review B, 90(20), 201112.
[34] Yvonnet, J., Chen, X., & Sharma, P. (2020). Apparent flexoelectricity due to heterogeneous piezoelectricity. Journal of Applied Mechanics, 87(11), 111003.
[35] Abdollahi, A., Domingo, N., Arias, I., & Catalan, G. (2019). Converse flexoelectricity yields large piezoresponse force microscopy signals in non-piezoelectric materials. Nature communications, 10(1), 1266.
[36] Codony, D. (2021). Mathematical and computational modeling of flexoelectricity at mesoscopic and atomistic scales (Doctoral dissertation, Universitat Politècnica de Catalunya).
[37] Wang, H., Jiang, X., Wang, Y., Stark, R. W., van Aken, P. A., Mannhart, J., & Boschker, H. (2019). Direct observation of huge flexoelectric polarization around crack tips. Nano letters, 20(1), 88-94.
[38] Buroni, J. L., Melnik, R., Rodríguez-Tembleque, L., Sáez, A., & Buroni, F. C. (2024). Closed-form expressions for computing flexoelectric coefficients in textured polycrystalline dielectrics. Applied Mathematical Modelling, 125, 375-389.
[39] Abdollahi, A., Vásquez-Sancho, F., & Catalan, G. (2018). Piezoelectric mimicry of flexoelectricity. Physical review letters, 121(20), 205502.
[40] Schiaffino, A., Dreyer, C. E., Vanderbilt, D., & Stengel, M. (2019). Metric wave approach to flexoelectricity within density functional perturbation theory. Physical Review B, 99(8), 085107.